Title

RAPID HEATING AND VAPORIZATION OF BINARY SOLIDS BY ABSORBING RADIATION II LASER PULSE VAPORIZATION OF URANIUM DIOXIDE

Authors

Tsai, C-h
Olander, D.R.

Publication Date

1983

LBL-15466
Preprint

Lawrence Berkeley Laboratory
UNIVERSITY OF CALIFORNIA

Materials & Molecular Research Division

Submitted to the Journal of Nuclear Materials

RAPID HEATING AND VAPORIZATION OF BINARY SOLIDS BY ABSORBING RADIATION II LASER PULSE VAPORIZATION OF URANIUM DIOXIDE

Chuen-horng Tsai and Donald R. Olander

January 1983

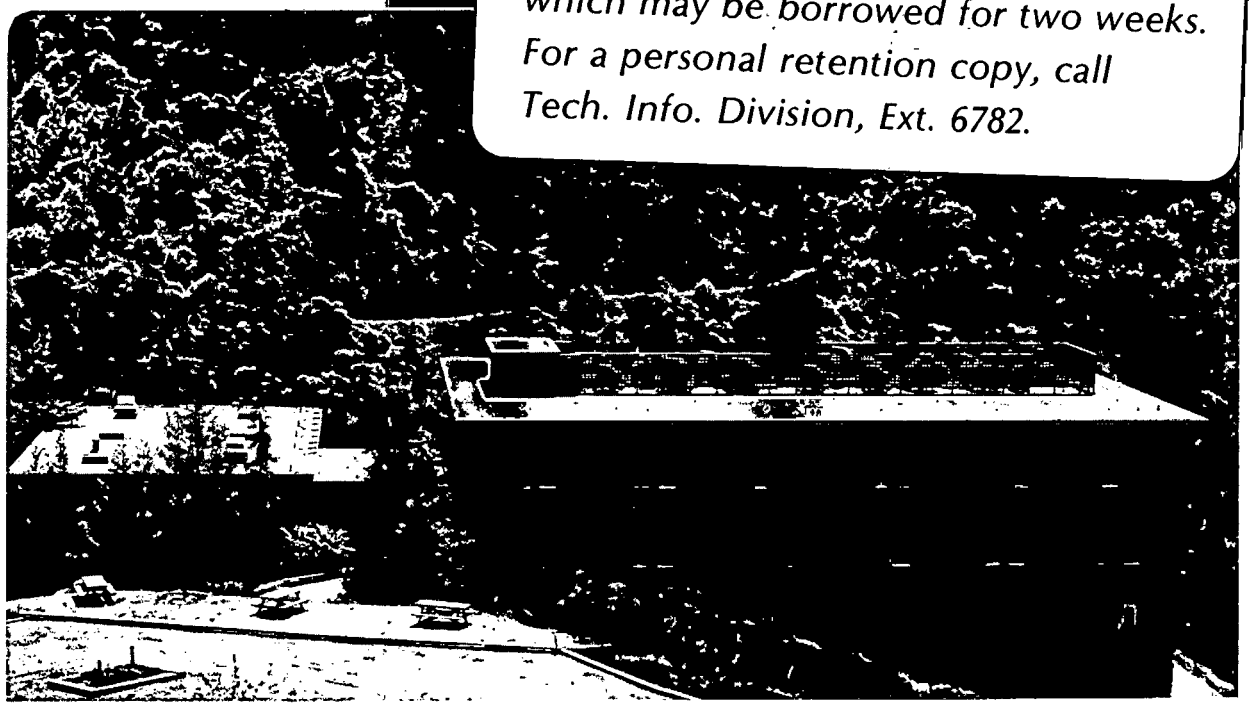

Prepared for the U.S. Department of Energy under Contract DE-AC03-76SF00098

DISCLAIMER

RAPID HEATING AND VAPORIZATION OF BINARY SOLIDS BY ABSORBING RADIATION

II LASER PULSE VAPORIZATION OF URANIUM DIOXIDE

Chuen-horng Tsai* and Donald R. Olander

Department of Nuclear Engineering

University of California

and

Materials and Molecular Research Division

Lawrence Berkeley Laboratory

Berkeley, CA 94720 U. S. A.

*Present address:

Dept. of Nuclear Engineering
National Tsing Hua University
Hsinchu, Taiwan
Republic of China

Abstract

Rapid heating of a small spot on a UO_2 specimen by a laser pulse generates a surface temperature excursion which was monitored by a fast-response automatic optical pyrometer. The maximum surface temperatures investigated ranged from $\sim$ 3700 K to $\sim$ 4300 K. The temperature transient vaporizes the surface and the vapor expands into vacuum. A quadrupole mass spectrometer was used to identify and analyze the species in the vaporizing flow and to measure the rate of evaporation from the surface. This information yielded the partial vapor pressure of each species and the composition in the vapor jet. The results were in fairly good agreement with thermochemical models based on extrapolation of low-temperature data. The degree of ionization in the hot vapor was estimated from the mass spectrometer measurement of ions and neutral molecules.

I INTRODUCTION

The analysis of a hypothetical core disassembly accident(HCDA) plays an important role in liquid metal fast breeder reactor safety assessments. The coupled neutronics--hydrodynamics computer code VENUS(1) is typical of such theoretical analyses. The peak fuel temperatures in these calculations vary from 4000 to 5000 K, a range of limited knowledge of fuel vapor properties, particularly its vapor pressure or equation of state. Extrapolations from static measurements performed well below the temperature range of interest are currently used in the HCDA analyses. The total vapor pressure data for UO_2 are in fair agreement up to the melting point (3130 K) but uncertainties approaching an order of magnitude appear at temperatures in the neighborhood of 5000 K (2). The composition of the high temperature vapor (i.e., its O/U ratio) is even less well established.

Equilibrium vapor pressure measurement techniques, such as Knudsen effusion and transpiration, cannot be used at very high temperatures not only because of the lack of suitable container materials for molten UO_2 but also because of departure from molecular evaporation, on which the Knudsen method depends(3). Moreover, even if obtainable, equilibrium vapor pressure data may not adequately represent the behavior of UO_2 during the rapid temperature excursion characteristic of an HCDA. These transients, which occur in tens of milliseconds, are probably better simulated by nonequilibrium experiments in which fuel vaporizes at surface recession rates of tens of centimeters per second into a low pressure background gas or into a vacuum. Several dynamic pulse techniques, including specimen heating by high energy electrons, neutrons, and laser beams, have been utilized in this type of experiment. Reviews of the various techniques are given in Refs. 4 - 6.

In the equilibrium technique and the electron- or neutron-heating methods, the composition of the condensed phase generating the vapor to be detected is well defined. In the laser method, on the other hand, only the surface of the specimen is heated. Not only are steep temperature gradients generated, but the high evaporation rates and the incongruent nature of UO_2 vaporization cause the composition of the evaporating surface to differ appreciably from that of the bulk solid. Moreover, just as the surface temperature changes with time during the heating pulse, so does the surface O/U ratio. In the present study, laser surface heating is used to achieve peak surface temperatures from 3600 to 4300 K. The surface temperature transient is followed experimentally by fast optical pyrometry. Unfortunately, no experimental method is available for the measurement of the surface O/U changes during the transient.

The vapor from the surface is emitted into a vacuum where it is analyzed by mass spectrometry. A direct line-of-sight quadrupole mass spectrometer located $\sim$ 40 cm from the heated spot on the UO_2 target detects the constituents of the vapor blowoff (U, UO, UO_2, and UO_3), whether as ions or neutral particles. The time-of-arrival of the various species at the mass spectrometer provides information on their ejection speeds. The magnitude of the mass spectrometer signal is related to the vaporization rate, and via the Hertz-Langmiur equation, to the vapor pressure. This method has been previously applied to iron and zirconium hydride by Olstad(7) and to graphite and alumina by Lincoln and Covington(8). In separate tests, some of the blowoff is collected on a series of disks positioned around the laser-irradiated spot to provide a measurement of the angular distribution of the evaporation process and to detect large particles leaving the surface.

II EXPERIMENTAL

II.1 Apparatus

The overall system diagram of Fig. 1 can be divided into five subsystems: the laser, the UO_2 target and the chamber in which it is housed, the mass spectrometer, the optical pyrometer and the transient data recorder. The summary of these components presented below may be supplemented by the detailed description given in Ref. 9.

The laser is Nd-glass, which delivers up to 30 J per pulse of 1.06 μm wavelength light. The output consists of a series of narrow spikes whose average trace is shown in Fig. 2. Due to the thermal inertia of the target material, the spikes merely create a ripple on the smooth temperature response which would result had the heat source actually been the curves of Fig. 2(8). There is a change in the laser firing characteristics at a pulse energy of $\sim$ 11 J, which accounts for the two curves in Fig. 2. These temporal shapes were measured using the beam splitter, magnesia diffuser and photodiode shown in Fig. 1. This subsystem also gives the total energy in each pulse, which must be reduced by the transmissivity of the focusing lens and the vacuum chamber window.

The radial distribution of laser power was determined by moving a razor blade across the focal plane at a 45^{o} angle by means of a micrometer and measuring the energy transmitted with a calorimeter. This information produced the normalized radial power distribution shown in Fig. 3.

The physics of the laser-solid interaction are controlled principally by the irradiance, or the power per unit area(10). The spot on the surface viewed by the mass spectrometer and the spot size of the optical pyrometer are small compared to the width of the focused laser beam (Fig. 3), so that

the system responds to the power density on the axis of the incident laser beam. The laser spot size was purposely not highly focused to avoid appreciable radial variation of laser power, which would have greatly complicated theoretical interpretation of the data. The variation of laser power with time, however, is quite nonuniform, as evidenced by the curves in Fig. 2. The temporal maximum of the power density q_p^{max} is related to the laser pulse energy E by(9):

$$q_p^{max} = \frac{E}{A_{eff} t_p} \qquad (1)$$

where $A_{eff} = 0.50\ cm^2$ is an effective laser spot size characteristic of the distribution in Fig. 3. The effective laser pulse duration is obtained by integration of the normalized curves shown in Fig. 2, which yields $t_p = 0.17$ ms for $E < 11J$ and $t_p = 0.21$ ms for $E > 11J$. For pulse energies of 10 and 30 J, q_p^{max} is $1x10^5$ and $3x10^5\ W/cm^2$, respectively. These values, in conjunction with the appropriate shape function from Fig. 2 and with reduction to accoun for reflection from the surface, provide the input surface heat flux needed for the theoretical calculations(11). A reflectivity of 0.17 has been taken from measurements of spectral emissivity(12).

The UO_2 sample is a 1.2 cm diameter, 1 mm thick wafer, the surface of which is polished to $\sim$ 6 μm roughness. It is mounted on a tungsten cap on the head of a electron bombardment heater in a vacuum of 10^{-7} Torr. The heater serves to heat the UO_2 up to 2045°C from mass spectrometer calibration and to preheat the sample to $\sim$ 1400°C, the ductile-to-brittle transition temperature(13), in order to avoid sample cracking resulting from the large thermal stress induced by laser heating; at this temperature, the light absorption cut-off of UO_2 is also shifted to wavelengths shorter than 1.06 μm, avoiding in-depth heating by radiation penetration

into the sample(14). The specimen was not pretreated to control stoichiometry; the theoretical analysis(11) indicates that the surface composition during the transient is affected principally by the incongruency of vaporization and little by the bulk O/U ratio.

The detector chamber is pumped to 10^{-10} Torr with the gate valve closed and to 10^{-8} Torr with it open. A quadrupole mass spectrometer is used to identify and analyze the various vapor species in the flow and to measure the density of each in the ionizer. The collimator in the target chamber (Fig. 1) limits the zone on the target with direct line-of-sight to the ionizer to a spot $\sim$ 1 mm in diameter.

The surface temperature transient is monitored by a fast-response automatic optical pyrometer focused to a spot on the target 1.73 mm in diameter. The pyrometer was calibrated with a 3000 K graphite blackbody source at the NASA-Ames Research Center. Standard procedures were used to extrapolate the calibration above 3000 K. The observed pyrometer response during a transient had to be corrected for time lags inherent in the external RC circuitry.

A transient waveform recorder is used to simultaneously record the signals from the laser power photodiode, the optical pyrometer, and the mass spectrometer.

II.2 Mass Spectrometer Calibration

The vapor in equilibrium with UO_2(s) is composed of UO_3, UO_2, UO, U, O and O_2, of which the first three are the most abundant. Prior to laser pulsing the UO_2 wafer is heated by the electron beam gun in the surface temperature range of 1760°C to 2045°C to generate a steady state molecular beam for both mass location and intensity calibration. The results plotted as log(ST) versus 1/T are shown in Fig. 4, where S is the signal from a

microammeter. From the slopes of the curves, heats of sublimation of 182.5 kcal/mol for UO_3 and 144 kcal/mol for UO_2 were obtained; the literature gives 143 kcal/mol for UO_2 (15). Since the slopes of the UO and U lines are close to that of UO_2, it is believed that they both represent the fragments of dissociative ionization (cracking) of UO_2 produced by impact with 70 eV electrons.

The ratios of the UO_3, UO and U signals to that of UO_2 in Fig. 4 can be expressed analytically as functions of the corresponding ratios of the electron multiplier efficiencies of the ions detected, the relative total ionization cross sections, the fragmentation pattern, and the ratios of the equilibrium pressures of the vapor species (9). The electron multiplier efficiencies were assumed to be proportional to the square roots of the ion masses and the relative ionization cross sections were taken from the work of Pattoret (16). The equilibrium pressures of the uranium-bearing species were calculated from the thermochemical model of urania proposed by Blackburn (17); the composition chosen at each temperature was that corresponding to congruent vaporization, which is the situation which is eventually attained in vacuum vaporization.

The congruently-vaporizing composition is that for which the O/U ratio of the evaporation flux is equal to that of the solid. This condition is expressed by the equation:

$$2 - x_c = \frac{3\Phi_{UO_3} + 2\Phi_{UO_2} + \Phi_{UO} + 2\Phi_{O_2} + \Phi_O}{\Phi_{UO_3} + \Phi_{UO_2} + \Phi_{UO} + \Phi_U} \qquad (2)$$

where Φ_i is the molar evaporation flux of molecular species i, which is given by the Hertz-Langmiur equation (Eq(1) of Ref. 11). These fluxes are functions of temperature and the O/U ratio of the solid, $2 - x_c$, which is

determined by iterative solution of the above equation. This calculation gives congruently-vaporizing compositions of 1.9991, 1.9981 and 1.9945 for 2100, 2300, and 2500 K, respectively.

Using the calibration data of Fig. 4, nine numbers describing the fragmentation pattern of the three gaseous oxides of uranium were deduced. These are shown in the form of a bar chart in Fig. 5, where the height of a segment of a bar represents the fraction of a particular neutral which fragments to the ion represented by the bar. This cracking pattern agrees quite well with the one determined by Pattoret(16). Figure 5 shows that only 8% of the UO_3 molecules ionize to produce the UO_3^+ parent ion. Ionization of UO_2 and UO, on the other hand, produces mainly the parent ion. However, the UO_2 equilibrium pressure is sufficiently larger than the UO pressure that the UO^+ signal is principally due to UO_2 fragmentation despite the 4:1 cracking pattern advantage for production of UO^+ from UO and UO_2 shown in Fig. 5. Similarly, even though neutral uranium atoms ionize solely to U^+, the density of U neutrals is so low that the observed U^+ signals in Fig. 4 are due entirely to fragmentation of the gaseous oxides.

In addition to determining the cracking pattern of the uranium oxides in the vapor phase, the calibration fixed the instrumental constant relating the output signal from the mass spectrometer to the number density of the species in the ionizer. This constant was used to convert signals recorded during the transient tests to the instantaneous number densities in the ionizer for comparison with theory.

III. RESULTS AND DISCUSSION

III.1 Surface Characterization

The laser-irradiated UO_2 sample surface was examined by scanning electron microscope. Fig. 6a shows a ring structure on the portion of surface within

the previously molten area. This pattern is attributed to radial propagation of capillary waves on the liquid surface driven by the recoil forces of the evaporating material(18).

Figures 6b and 6c show high-magnification views of the surface inside and outside, respectively, of the previously molten zone. Despite rapid solidification following the pulse, the grain size in Fig. 6b is just a bit smaller than in the unmelted material shown in Fig. 6c. However, the fact that both surfaces exhibited distinct grains without special preparation is evidence of thermal etching.

The white dots decorating the grain boundaries on the previously molten surface may represent precipitated metallic uranium. The kinetic analysis of the surface composition evolution(11) indicates that substantial hypostoichiometry should have occurred during the pulse. For the laser energy which produced the surface features in Fig. 6, the minimum O/U of the surface is calculated to be 1.78. However, the temperature is also very high and if thermochemical models(17) are applicable at $\sim$ 4000K, the surface should have remained in the single-phase region during the entire transient. The grain boundary particles and the grain surfaces were examined by scanning Auger microscopy to determine the composition. The dots and the matrix both gave essentially identical Auger electron spectra. The identity of the particles thus remains unsure, although the most likely assignment is still precipitated uranium metal.

Figure 7 shows a profilometer trace of the original surface and the crater produced by 5 laser pulses each of 28 J on the same spot. The crater size corresponds to loss of $\sim$ 55 mg of UO_2. The calculated mass loss(11) for the 5-shot sequence is 8 mg. This discrepancy may be due to "chunk" sputtering(10) or to microexplosions caused by subsurface porosity(19).

III.2 Collection of Emitted Material

In order to better understand the vaporization process, the target was surrounded with semicircular arrays of small disks to catch some of the vaporized UO_2. Two arrays of disks were used, one set of teflon and the other of aluminimum.

Following the laser pulses, the teflon disks were irradiated in a reactor in order to determine the quantity of uranium on them by neutron activation. The variation in radioactivity with the angle from the target normal provides a direct measure of the angular distribution of the vaporized material from the laser spot. Fig. 8 shows the angular distributions normalized with respect to the total amounts of material evaporated. The triangles show the results for five 28 J laser shots with the collectors arranged in a semicircle contained in a plane at right angles to the plane of the laser beam and the target normal. This series of shots produced the crater shown in Fig. 7. Integration of the angular distribution gives a total of 9 mg of UO_2 evaporated, which compares favorably with the theoretical value of 8 mg calculated from the model of Ref. 11. The circles in Fig. 8 are the results from two 26 J laser shots with in-plane collectors. In this case, 4 mg of UO_2 were collected, which is the same quantity predicted to evaporated by the theoretical model. Also shown on Fig. 8 are $\cos\theta$ and $\cos^2\theta$ distributions suggested for Knudsen effusion and supersonic free-jet expansion respectively. The angular variation of the mass flux can be approximated by $\cos^n\theta$ distribution where n is close to one.

The aluminum disks were used to collect some of the vapor plume from the 5-shot test series for scanning electron microscope examination. This test was intended to determine whether the vapor blowoff consisted solely

of a molecular vapor or also contained a condensed phase. The SEM micrographs in Fig. 9, show condensed-phase agglomerates of UO_2 on the disks. Some are donut-shaped and some spherical, suggesting that they were liquid globules before striking the disks. The radii of the frozen droplets range from 1 μm to 15 μm. Elemental analysis (EDAX), also shown in Fig. 9, reveals that they are principally uranium, most likely in the form of UO_2. Two interpretations of this result are possible: either UO_2 liquid droplet ejection occurs directly from the melt, or liquid droplets are formed by condensation in the highly supersaturated vapor plume. The mass associated with the particles (estimated from the optical microscope observation) is at most 1% of the total UO_2 collected on each disk, so that the frozen droplets cannot account for the excessive mass loss inferred from the crater volume. Therefore, the formation of liquid droplets does not affect the angular distribution measurement, nor the interpretation of vaporization as a molecular process.

III.3 Surface Temperatures

Since the thermal response of the laser-irradiated surface can be measured (by optical pyrometry) and calculated (by the method described in ref. 11), independent check of theory with experiment is available. Figure 10 shows such a comparison for a 10 J laser pulse. The experimental temperature trace rises more rapidly than the calculated thermal transient, but the maximum surface temperature and the cooling rate are well-predicted by the theory. The time offset of the maximum temperature, however, is significant and was observed in all shots. No reasonable changes in the RC time constant of the pyrometer's external circuitry could rectify the discrepancy, nor could substantial alterations in the thermal properties of UO_2 used in the calculations of the surface temperature appreciably shift the position of the theoretical maximum.

Figure 11 shows the experimental and computed temperature maxima for all six shots. The experimental scatter is appreciable; for the three shots with laser energies between 10.2 and 10.6 J, the observed maximum temperatures range from 3770 to 4090 K. However, the data clearly follow the predicted trend with respect to laser energy. The dashed lines in Fig. 11 represent the uncertainty band associated with the use of imperfectly known thermal properties of UO_2 in the theoretical calculation(11).

III.4 Molecular Densities in the Vapor

The mass spectrometer signals were recorded for six series of four laser shots each. In each series, the laser pulse energy was kept constant and in each shot of a series, a different mass, corresponding to the vapor species U, UO, UO_2 and UO_3, was monitored. Masses corresponding to the dimers of UO and of UO_2 were examined, but no signals were found. Figure 12 shows the raw signals for the UO_2^+ following a laser shot. For comparison with theory, the signals from the mass spectrometer needed to be converted to molecular densities of vapor species in the ionizer region. Such a conversion required several corrections to the raw data. First, the mass spectrometer instrumental constant and the effects of fragmentation by electron impact had to be taken into account; this was accomplished using the results of the steady state calibration described in Section II.2, and Fig. 5 in particular. Second, the time constant associated with the resistance and capacitance of the electronic circuitry following the electron multiplier needed to be incorporated into signal analysis in a similar manner to that applied to the pyrometer output. Third, a correction for the drift time of ions down the analyzing section of the mass spectrometer was included. These procedures(9) permitted conversion of the mass spectrometer signal response such as that shown in Fig. 12 to $n_i(t)$, the density of neutral species i in the ionizer as a function of time following initiation of the

laser pulse. The first (smallest) spike in Fig. 12 is an artifact, the second is due to ion emission and will be considered in the following section, and the third and largest pulse is the neutral species output which leads to the solid curve in Fig. 13 when all corrections are applied. The peaks of the molecular density curves are substantially delayed from the peaks of the laser pulses (Fig. 2) because of the 40 cm flight path traversed by the molecules evaporated from the surface.

One of the major objectives of this study is to relate the experimental molecular density curves to the vapor pressure of each species at the temperature and composition conditions of the surface. Theoretically, such a connection consists of two parts. First, the vaporization rate from the surface needs to be related to surface temperature and surface composition via the equilibrium vapor pressure. Second, the net vapor flux from the surface must be converted to a molecular density at an arbitrary downstream position.

The rate of vaporization is assumed to be given by the Hertz-Langmiur formula, which was originally deduced for low-rate vacuum vaporization. However, as explained in Ref. 11, it applies even when the evaporation rate is sufficiently large to create a collision-dominated vapor cloud near the surface, provided that backscattering of evaporated molecules from the dense gas is accounted for. Fortunately this backscattering correction is independent of gas conditions, so the vaporization rate is unaffected by the expansion of the vapor cloud downstream of the surface.

With the flux from the heated spot on the surface specified, the molecular density along the centerline of the expansion depends only upon the angular distribution of the emission and on the speed distribution of the molecules. These features of the expansion depend upon whether the vapor leaves the surface in free-molecular flow or as a collision-dominated flow analogous to

gas issuing from an orifice. In the former instance, the angular distribution varies as $\cos\vartheta$, where ϑ is the angle from the surface normal, and the speed distribution is that of a Maxwell-Boltzmann gas at the instantaneous temperature of the surface. Detailed models of the collisional or gasdynamic expansion process have been presented(4,6), but determination of the number density from the source flux does not depend sensitively upon these details. Generally, the gasdynamic models give an angular distribution which is proportional to $\cos^2\vartheta$, which tends to increase the number density along the centerline for a given evaporation flux. In addition, these models predict terminal Mach numbers of the expansion which are greater than unity, which acts to reduce the number density for a fixed flux because the molecules are moving faster than if they possessed the thermal velocities characteristic of the hot surface. These two differences between the gasdynamic expansion and free-molecule evaporation tend to cancel insofar as determining the vapor density is concerned.

Thus, the free-molecule flow model is used to connect surface evaporation rates to downstream molecular densities, with the realization that the calculation could be somewhat in error because of incorrect angular and speed distributions. However, these discrepancies are believed to be minor compared to the general precision of the experimental method. As summarized in Ref. 7, the molecular density of species i in the ionizer located a distance ℓ from a heated spot of area A which is subjected to a temperature transient $T_s(t)$ is given by:

$$n_i(t) = \frac{\alpha_i(1-\beta)\ell A}{k}\left(\frac{m_i}{2\pi k}\right)^{3/2}\int_0^t \frac{P_i(T_s,x_s)}{T_s^{5/2}(t-\tau)^4}\exp\left(\frac{-m_i\ell^2}{2kT_s(t-\tau)^2}\right)d\tau \qquad (3)$$

where P_i is the equilibrium vapor pressure of species i, and is a function

of surface temperature T_s and surface composition x_s. The mass of the molecule is denoted by m_1 and k is Boltzmann's constant. The evaporation coefficient α_i is assumed to be unity for all species emitted from hot UO_2, which appears to be a reasonable approximation for this type of material(11). The gasdynamic backscattering factor β is taken to be 0.18(11). The area A is defined by the geometry of the flight path between the surface and the mass spectrometer ionizer and the dimensions of the collimator in Fig. 1. As shown in Fig. 3, the laser intensity varies very little over the spot on the surface viewed by the mass spectrometer ionizer. Equation (3) is a convolution integral summing all contributions to the molecular density in the ionizer at time t after initiation of the laser pulse due to molecules emitted from the surface at times τ which cover the entire range from 0 to t. The integrand essentially represents the probability that a molecule emitted at time τ will have the correct speed (and hence transit time) to arrive at the ionizer at time t.

There are two ways of utilizing Eq(3) for comparing data with theory. The first method consists of using one of the thermochemical models of UO_2 derived from low-temperature measurements to predict the equilibrium pressure P_i. Using this to calculate the theoretical molecular density transient by Eq(3), either the measured or the calculated temperature transient $T_s(t)$ can be used. However, the surface composition transient $x_s(t)$ can only be calculated. An example of this approach is illustrated in Fig. 13, in which the normalized vapor density curve for the vapor species UO_2 obtained from the experiment is compared with the computed response for the same species. The latter was determined from Eq(3) using Blackburn's model(17) of the UO_2 pressure; surface temperature and composition were computed by the technique of Ref. 11. Although the shapes of the distributions are remarkably similar for theory and experiment, the maxima differ by 0.25 ms. The arrow shown in Fig. 13 is the time-of-arrival corresponding to the maximum molecular density

as predicted by a gasdynamic model(20). The discrepancy in the time of the peak density between this theoretical model and the experiment is even greater than that for the free molecule evaporation model. In addition, the width of the time-of-arrival distribution computed from the gasdynamic model(not shown on Fig. 13) is narrower than that of the data or of the free molecule model.

Figure 14 compares the maximum density of the UO_2 time-of-arrival curves for six laser shots covering a two-fold range in energy with the theoretical predictions using the same basis of that employed in preparing Fig. 13. The break in the line is due to the change in laser characteristics at a pulse energy of 11J (see Fig. 2).

The low-temperature thermochemical models give the pressures of all species (i = U,UO,UO_2 and UO_3), which provides another means of comparing theory with experiment. Because the data for U,UO and UO_3 are sensitive to the fragmentation pattern due to electron impact in the mass spectrometer, they are not as reliable as the UO_2 results, which are relatively free from this complication. For example, U^+ arises nearly entirely from fragmentation of UO_2 which is present at four orders of magnitude higher density. In addition, the results for UO_3 are more reliable than those of UO because the UO_3^+ signal represents only parent ions. With these caveats in mind, Table 1 compares the experimental results and theoretical predictions of the ratios of the maximum molecular densities of UO_3 and UO relative to UO_2 for the six series of laser shots. Of the three models examined, those of Blackburn(17) and Breitung(21) are consistent with the experiments. The Green-Leibowitz model (22) predicts a higher fraction of UO_3 in the vapor than observed.

In reactor safety applications, the UO_2 equation of state usually appears as a pressure-temperature relation. This suggests an alternative means of

comparing the present data with previous work at low temperature. The laser/mass spectrometer data for a particular species (say the dominant UO_2 molecule) are used in the left hand side of Eq(3) and a P-T relation chosen for the integrand on the right hand side to best fit these data. To reduce the computations required, fitting is done with the maximum UO_2 densities shown in Fig. 14 rather than some other feature of the time-of-arrival curve (such as its area). The form of the vapor pressure equation is:

$$\log P = A + B/T + C\log T \qquad (4)$$

where the constants A, B and C are chosen by the fitting process. The results of this procedure depend upon the surface temperature history $T_s(t)$ used in the integral of Eq(3). As illustrated by Fig. 10, the observed and calculated surface temperatures differ in shape, and this difference is reflected in the constants of the vapor pressure formula determined by data fitting. Because of this uncertainty in temperatures, the results of the fitting process are shown in Fig. 15 as a band. The upper limit of the dotted area represents the vapor pressure for formula determined on the basis of calculated surface temperatures and the lower limit of the band corresponds to the use of measured surface temperature histories in the data fitting process. Also shown on Fig. 15 is the UO_2 pressure computed from Blackburn's model(17). The uncertainty band in the urania total (not UO_2) pressure recommended by the IAEA working group(2) is also shown in Fig. 15. The present data fall on the low side of this band.

Because of the incongruency of urania vaporization, the O/U ratio of the vaporizing surface was well below two. The data band in Fig. 15 therefore represents evaporation of highly hypostoichiometric urania. However,

theoretical models of urania thermochemistry indicate that the total pressure (and probably that of UO_2 also) is not sensitive to the O/U ratio(22).

III.5 Degree of Ionization of the Vapor

Neglecting the small blip on the left hand side of the trace in Fig. 12, two time maxima are detected for all the species except UO_3, for which the ion signal is probably too small to be measurable. The first peak is believed to arise from hot ions emitted with the vapor cloud because it persists when the filament current in the ionizer is turned off. Without an ionizing electron current the larger second peak in Fig. 12 disappears.

The degree of ionization of the hot vapor can be estimated from the double-peaked mass spectrometer signals. The relative magnitudes of the raw signals in Fig. 12 do not directly reflect the ion content of the vapor because the mass spectrometer does not have the same efficiences for ions as for neutral molecules. The ionization fraction for neutral molecules in commercial quadrupole mass spectrometers is of the order of 10^{-4} while that for ions is by definition unity. An efficiency of ion extraction less than unity results from the fact that the beam enters the mass spectrometer ionizer (whether as ions or as neutrals) at right angles to the axis of the quadrupole structure(23). Because of this configuration, rapidly moving ions are not as easily extracted as the more slowly moving neutrals which are ionized by electron impact. The thermal molecules emitted from the surface have translational energies corresponding roughly to that of an equilibrium gas at $\sim$ 4000 K, or about 0.35 eV.

Estimation of the energy of the ions contained in the emitted vapor is more difficult. Ion production due to bombardment of solids by Q-switched lasers is well established, and is in fact the basis of commercial laser

ion source mass spectrometers(24). For peak laser intensities of 10^9 - 10^{10} W/cm^2, ions with energies up to $\sim$ 1000 eV have been observed, with fairly narrow energy distributions(25). For high mass materials, the average ion kinetic energy varies approximately as the 1/3 power of the laser intensity(10), at least in the Q-switched intensity range. Extrapolating down to the range of 10^5 - 10^6 W/cm^2 peak intensities characteristic of the normal mode pulses used in this work, the average energy of the ions in the vapor is estimated to be 30 eV. This order of magnitude estimate of ion energies is supported by the observed delay times between the ion peak and the initiation of the laser pulse. The ion flight time is shown in Fig. 16 for the UO^+ signal recorded with the ionizer current in the mass spectrometer shut off. The 0.15 ms delay between the ion arrival curve and the laser irradiation curve corresponds to the transit time of UO^+ ions of 11 eV energy. In similar tests, the times of arrival of the maximum ion signals for U^+, UO^+ and UO_2^+ were found to vary as the square root of the ion mass. Because the ionizer cage of the mass spectrometer is held at 11 V above ground potential during normal operation, the ions entering the extraction region of the instrument have translational energies of $\sim$ 20 eV if the 30 eV estimate based on peak laser intensity is accepted. In addition, ions with energies less than 11 eV will not reach the detection system at all. Very fast ions will pass through the ionizer cage without being extracted into the quadrupole structure.

Assuming that the ion and neutral signals recorded by the mass spectrometer correspond to translational energies of 20 and 0.35 eV, respectively, the extraction efficiences are estimated from the method presented in Ref. 23 to be 1% and 80%, respectively. Combining these

figures with the ionization efficiencies of the neutrals (taken to be 10^{-4}) and for the ions (unity), the latter are detected with an efficiency which is $(10^{-2}/0.8)\ (1/10^{-4}) = 125$ times greater than the former. Rough estimates of the areas under the ion and neutral peaks in Fig. 12 shows the former to be ~6% of the latter. Taking into account the relative detection efficiencies, the fractional ion content of the vapor is found to be 5×10^{-4}. This value is much smaller than the ~2% calculated degree of ionization reported by Karow(26), which is based on Saha's equation applied to an effective unisolated ionization potential. However, because of the very approximate nature of the detection efficiency of neutrals and the inability of the detector to respond to low and high energy ions, the experimental ion fraction in the hot vapor is a lower limit on the actual value. By way of comparison, ion fractions produced from normal mode laser pulses of the type used here are reported by Kovalev, et al,(25) to range from 10^{-5} up to $\sim 10^{-2}$.

Although there are theoretical grounds for rationalizing the observed fraction of ions observed in the ejected vapor, the very high energies of these ions compared to thermal energies (defined by the ~ 4000 K neutrals) is difficult to understand. Whether the source of the ions is thermionic emission from the surface, as suggested by Ready(10), or gaseous ionization as assumed by Karow(26), the resulting ions should share the thermal energy of the rest of the vapor. However, the ions detected in the experiments are clearly not in thermal equilibrium with the neutral molecules emitted from the surface. It is possible that the electrons in the vapor cloud are accelerated to sufficiently high energies by the electromagnetic field of the incident laser light to transfer tens of electron volts of kinetic energy to ion with which they collide.

IV. CONCLUSIONS

The mass spectrometric technique is the only way of identifying and measuring the evaporation rates of different species from vaporizing solids. The time-of-arrival curves permit estimation of the velocity of the blowoff, thus providing a way of directly checking whether transient vaporization is an equilibrium process. The results of the vapor pressure and the vapor composition for UO_2 deduced from the present experiments generally support existing thermochemical models for calculating the equilibrium partial pressure of each species by extrapolation of low-temperature measurements. The good accord also suggests that equilibrium vaporization, after taking into account the oxygen depletion of the surface, successfully describes the vaporization process in the sub-millisecond transient. The transient calculation presented in Ref. 11 is more suitable than either the congruent or the "forced congruent"(27) calculations for this purpose.

Comparison of the measured time-of-arrival and the width of the mass spectrometric signals to the free molecule (collisionless expansion) and gasdynamic (collision-dominated continuum flow) models suggests that the former best represents the blowoff process in vacuum. This observation is the opposite of that made by Lincoln and Covington (8) who, in a similar experiment with other materials (graphite and alumina), measured terminal Mach numbers considerably larger than one.

The mass spectrometric measurement also provides a very approximate measure of the degree of ionization of the high temperature vapor ejected from the surface. The experimental result is lower than the calculation based on Saha's equilibrium model, but the experimental technique may have missed large numbers at low energy ions.

Acknowledgement

The authors would like to acknowledge Dr. Alan Covington of the Ames

Research Center of National Aeronautics and Space Administration for valuable scientific and technical assistance throughout this work. This work has been supported by the Director, Office of Energy Research, Office of Basic Energy Science, Materials Science Division of the U. S. Department of Energy under contract No.

TABLE 1

The Ratios of Maximum UO_3 and UO Densities to those of UO_2

laser energy (J)	$n_{UO_3}^{max} / n_{UO_2}^{max}$				$n_{UO}^{max} / n_{UO_3}^{max}$			
	Theory (17)	Theory (21)	Theory (22)	Exp	Theory (17)	Theory (21)	Theory (22)	Exp
10.6	.13	.29	.97	.10	.16	.22	.008	.28
10.3	.14	.32	1.00	.15	.13	.19	.007	.24
11.4	.14	.30	.95	.13	.13	.22	.008	.10
16.8	.10	.22	.75	.07	.31	.49	.015	.22
7.3	.20	.38	1.16	.22	.05	.11	.004	.06
10.2	.14	.31	.99	.12	.13	.20	.007	.28

REFERENCES

1. S. Aoi, T. Sawada, M. Fukuda and T. Naganuma, "VENUS-PM: An Analytical Investigation of a Core Disassembly Process in Fast Reactors," SJ-206-76-25 Tr, JAPFNR-308, Oct. 1976.
2. IAEA Specialists' Meeting on Equations of State of Materials Relevance to the Analysis of Hypothetical Fast Breeder Reactor Accidents, IWGFR/26, Harwell, UK, June 1978.
3. R. J. Ackermann, E. G. Rauh and M. H. Rand, IAEA Symposium on Thermodynamics of Nuclear Materials, Vol. I, Paper IAEA-SM-236/59, Julich, 29 Jan. - 2 Feb., 1979.
4. M. Bober, W. Breitung, H. U. Karow, H. Kleykamp, G. Schumacher and K. Thurnay pg. 8 of Ref. 2.
5. W. Breitung, "Vapor Pressures of Oxide Reactor Fuels above 3000 K: Review and Perspective", NUREG/CR-2261 (1981).
6. R. W. Ohse, J. F. Babelot, C. Cercignani, P. R. Kinsman, K. A. Long, J. Magill and A. Scotti, J. Nucl. Mater. 80 (1979) 232.
7. R. A. Olstad and D. R. Olander, J. Appl. Phys. 46 (1975) 1499, 1509.
8. K. A. Lincoln and M. A. Covington, Int. J. Mass Spectrometry & Ion Physics, 16 (1975) 191.
9. C. H. Tsai, "The Kinetics of Laser Pulse Vaporization of UO_2 by Mass Spectrometry," Ph.D. Thesis, University of California, Berkeley, LBL-13679, 1981.
10. J. F. Ready, "Effects of High Power Laser Radiation", Academic Press, 1971.
11. C. H. Tsai and D. R. Olander, Part I of this series.
12. M. Bober and H. U. Karow, 7th Symp. on Thermodynamical Properties, NBS, Washington, D. C., 1977.

13. D. R. Olander, Fundamental Aspects of Nuclear Reactor Fuel Elements, Chap. 16, ERDA Technical Information Center, Oak Ridge, Tennessee, Apr. 1976.

14. M. J. Davies, Ph.D. Thesis, Dept. of Inorganic and Structural Chemistry, University of Leeds, Jan. 1970.

15. M. Tetenbaum and P. D. Hunt, J. Nucl. Mater. 34 (1970) 86.

16. A. Pattoret, Ph.D. Thesis, Université Libre de Bruxelles, 1969, pp. 30-36.

17. P. E. Blackburn, J. Nucl. Mater. 46 (1973) 244; private communications, 1975/76.

18. J. Magill and R. W. Ohse, J. Nucl. Mater. 71 (1977) 191.

19. R. W. Ohse, P. G. Berrie, H. G. Bogensberger and E. A. Fischer, IAEA Symposium on Thermodynamics of Nuclear Materials, Paper IAEA-SM-190/8, Vienna Oct. 1974.

20. F. Tehranian, "A Gasdynamic Model of Rapid Evaporation of a Solid into a Vacuum", unpublished report (1982).

21. W. Breitung, "Calculation of Vapor Pressures of Oxide Fuels up to 5000 K in Equilibrium and Nonequilibrium Evaporation", KfK 2091 (1975).

22. D. W. Green and L. Leibowitz, J. Nucl. Mater. 105 (1982) 184.

23. W. J. Siekhaus, R. H. Jones and D. R. Olander, J. Appl. Phys., 41 (1970) 4392.

24. R. J. Conzemius and J. M. Capellen, Inter. J. Mass Spec. & Ion Phys. 34 (1980) 197.

25. I. D. Kovalev, G. A. Maksimov, A. I. Suchkov and N. V. Larin, Inter. J. Mass. Spec. & Ion Phys., 27 (1978) 101.

26. H. U. Karow, KfK - 2390, Feb. 1977; Rev. Int. Hautes Temper. Refract Fr., 15 (1978) 347.

27. W. Breitung, "Evaporation Kinetics of Oxide Fuels and Their Consequences on Actinide Redistribution in Reactor Fuel Pins and on Fuel Vapor Pressures Under Conditions of Core Disruptive Accident", KfK-2240 (1976).

FIGURE CAPTIONS

1. Apparatus for detection of laser-induced vaporization by mass spectrometry
2. Time dependence of the laser power
3. Radial dependence of laser power; spots viewed by: (a) the mass spectrometer and (b) the optical pyrometer
4. The mass spectrometer signals for steady state vacuum vaporization of stoichiometric urania
5. Fragmentation pattern of gaseous uranium oxide for 70 V electrons
6. Scanning electron microscope images of the surface of laser-irradiated UO_2
7. Profilimeter trace of UO_2 surface after five 28J laser shots on the same spot
8. Angular distribution of the laser blow-off.
9. Aluminum disk collector surface following five shots of 28J on a UO_2 target (a), (b) Scanning electron microphotographs, (c) EDAX analysis of the white spot in (b)
10. Surface temperature transient following a 10J laser pulse
11. Maximum surface temperatures
12. UO_2^+ oscilloscope signal from mass spectrometer; vertical: 0.1 volts/div and horizontal: 1 ms/div
13. Normalized UO_2 molecular density: from mass spectrometer signal (solid line); free-molecule flow model (dashed line); gasdynamic expansion model (arrow)
14. Maximum UO_2 molecular density in the mass spectrometer ionizer

15. The pressure - temperature relation for UO_2

——— Blackburn's model for UO_2 partial pressure (17)

----- Recommended limits of total vapor pressure (2)

 This work.

16. Laser and mass spectrometer signal for UO^+ with no ionizing electron current

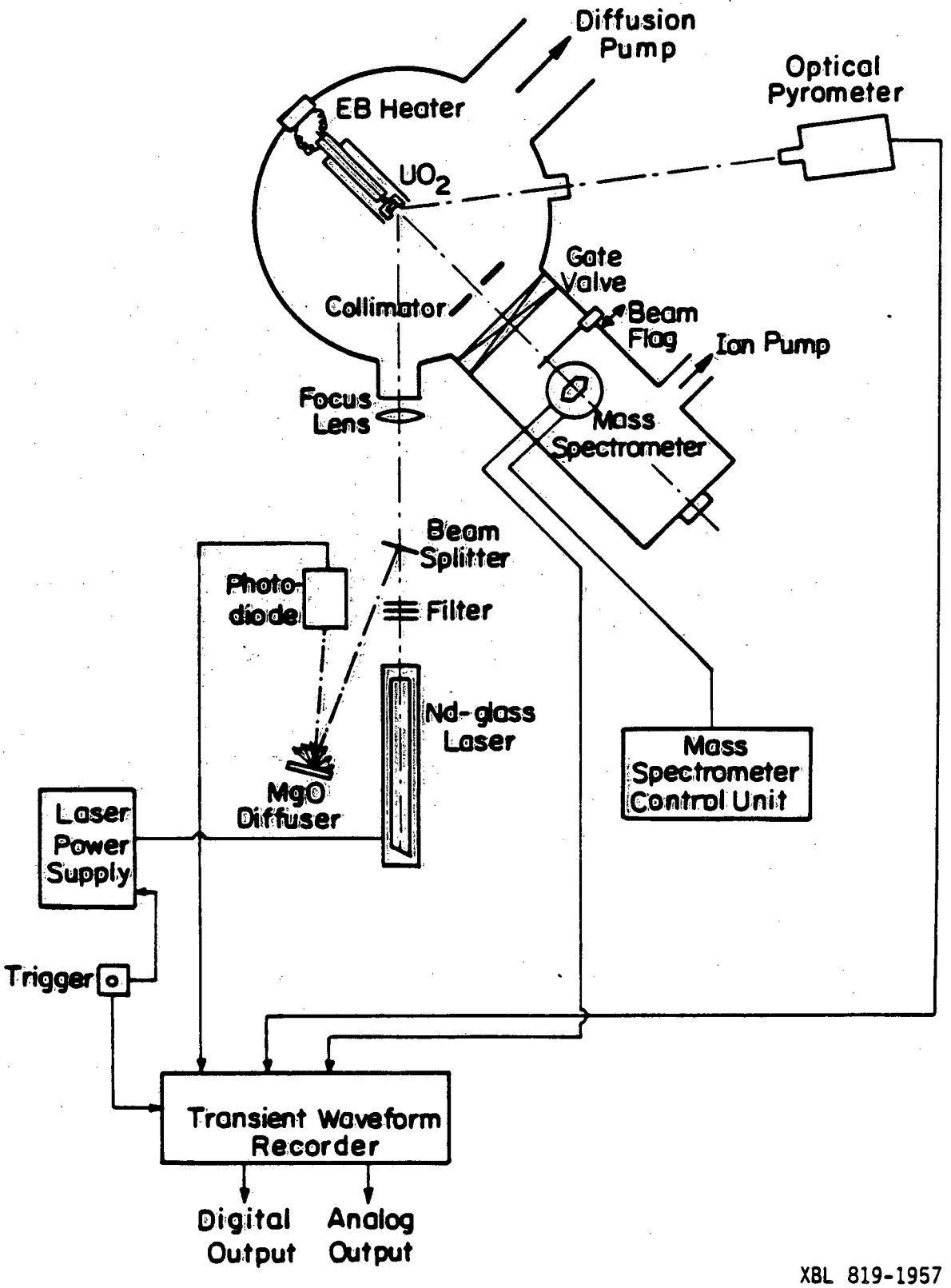
Diffusion Pump
Optical Pyrometer
EB Heater
UO_2
Gate Valve
Collimator
Beam Flag
Ion Pump
Focus Lens
Mass Spectrometer
Beam Splitter
Photo-diode
Filter
Nd-glass Laser
MgO Diffuser
Mass Spectrometer Control Unit
Laser Power Supply
Trigger
Transient Waveform Recorder
Digital Output
Analog Output
XBL 819-1957

Fig. 1

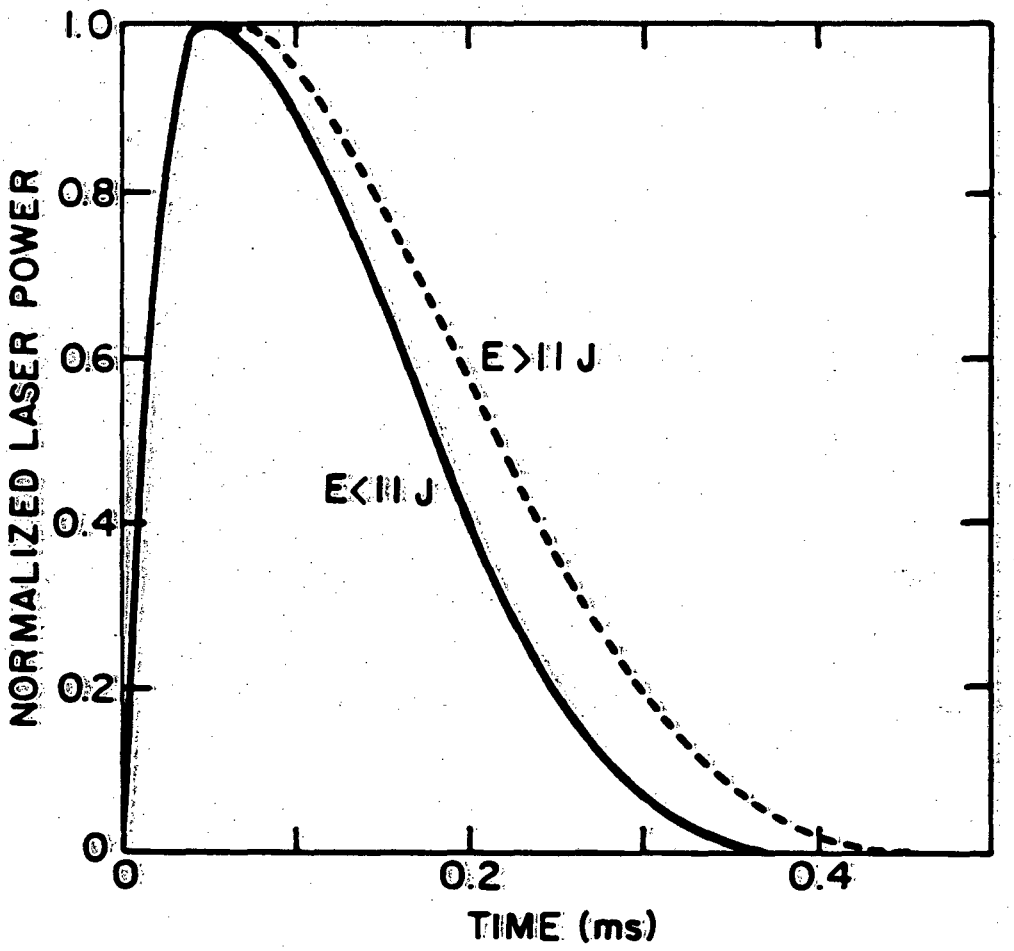
NORMALIZED LASER POWER
1.0
0.8
0.6
0.4
0.2
0
0
0.2
0.4
TIME (ms)
E>11 J
E<11 J
XBL8111-12521

Fig. 2

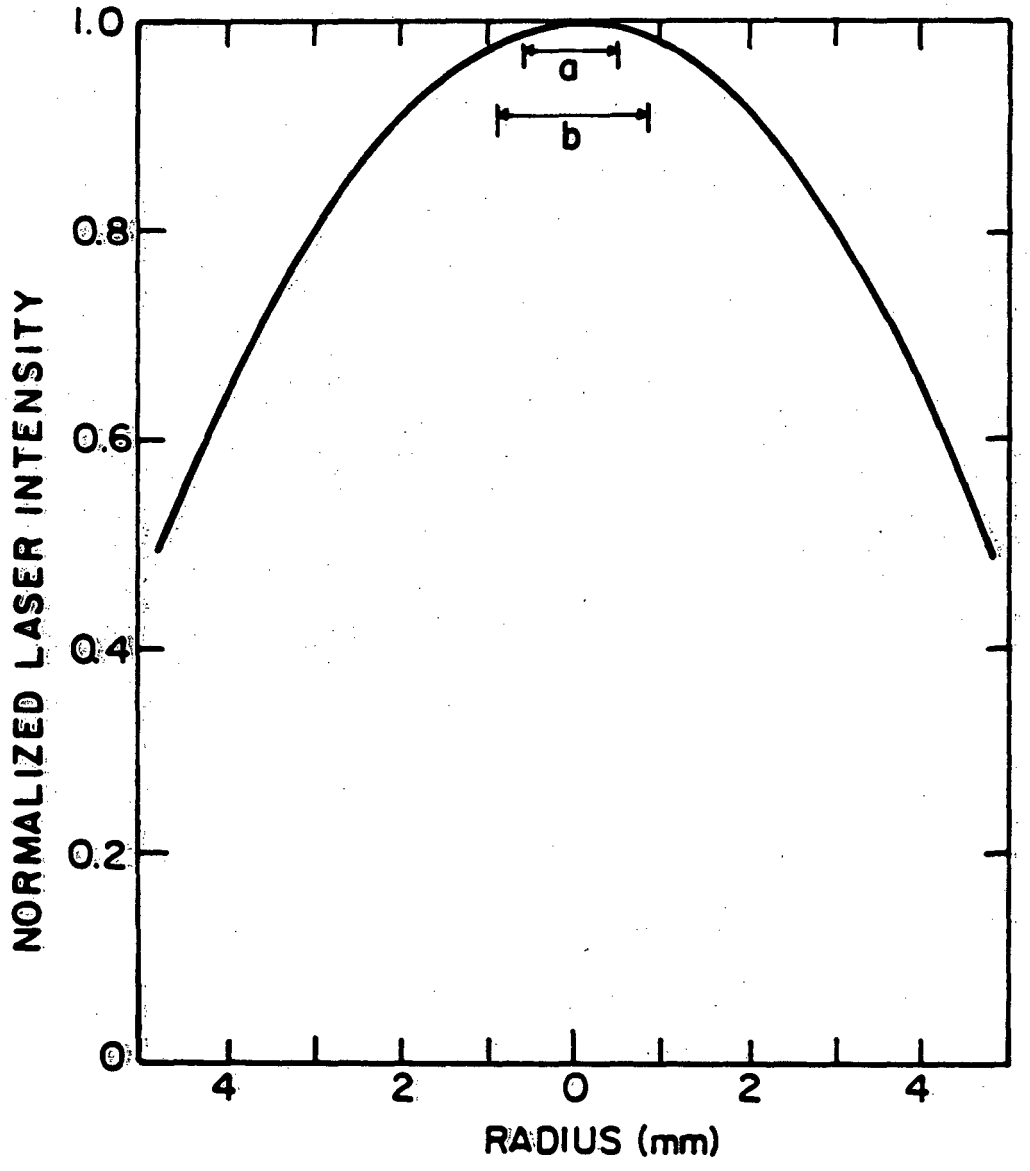
1.0
0.8
0.6
0.4
0.2
0
a
b
NORMALIZED LASER INTENSITY
4
2
0
2
4
RADIUS (mm)
XBL 8111-12508

Fig. 3

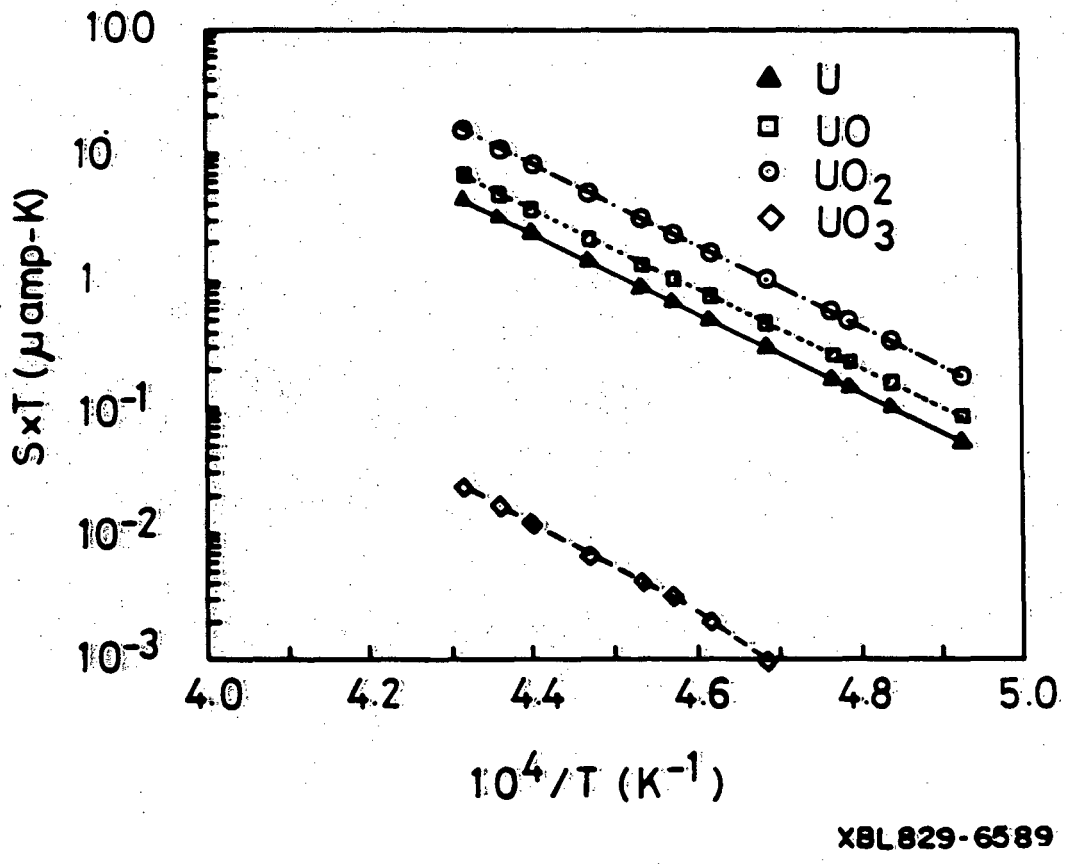

Figure 2.4

Fig. 4

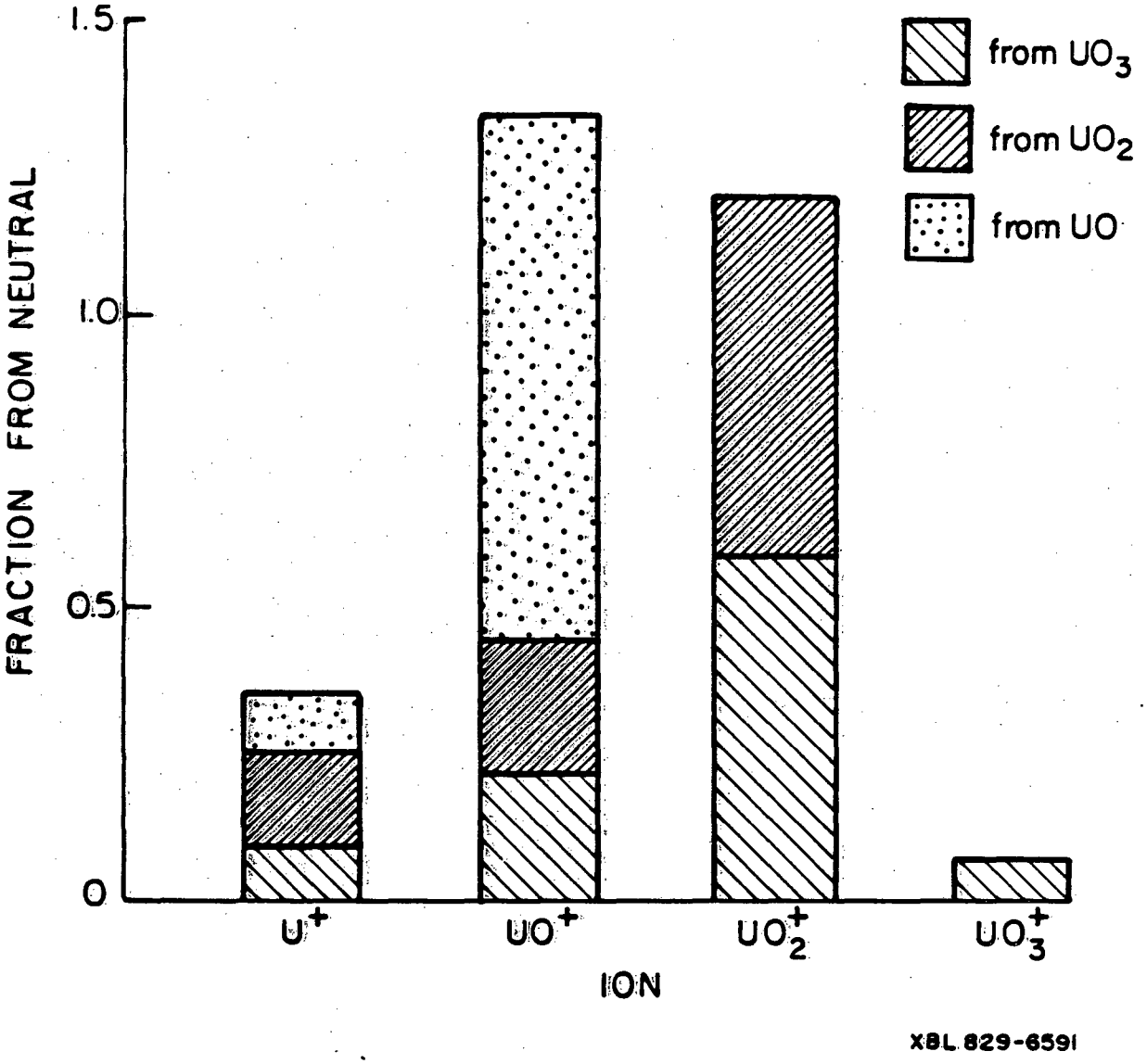
1.5
1.0
0.5
0
FRACTION FROM NEUTRAL
from UO_3
from UO_2
from UO
U^+
UO^+
UO_2^+
UO_3^+
ION
XBL 829-6591

Fig. 5

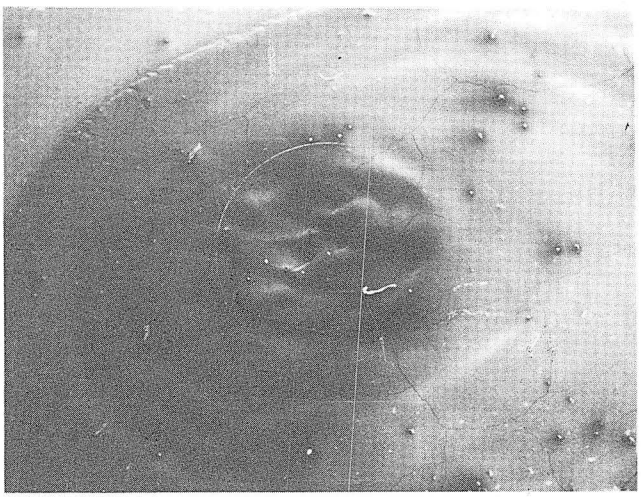

(a)

1000 μm

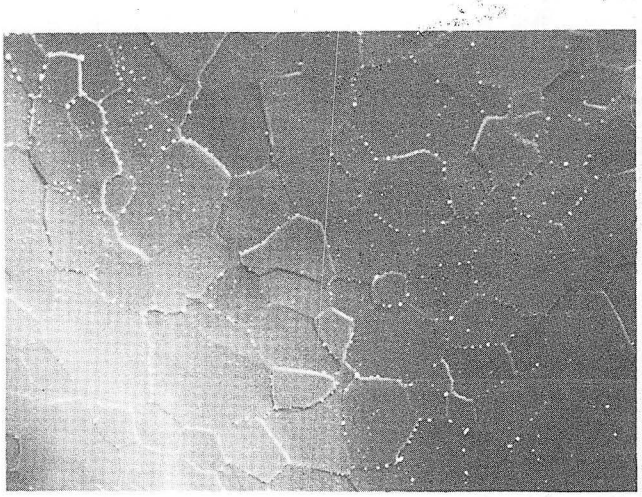

(b)

10 μm

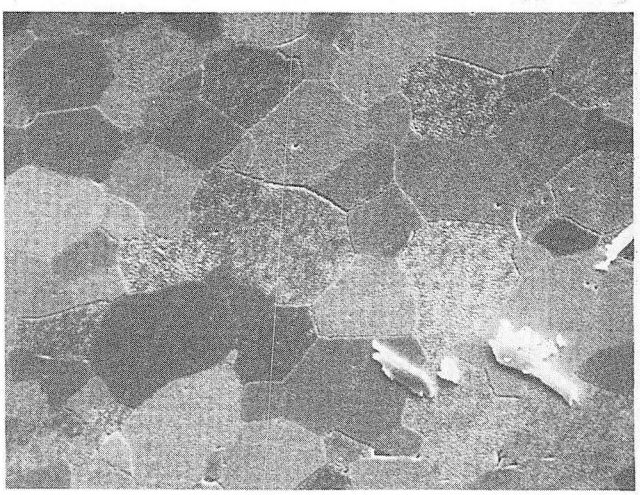

(c)

10 μm

Fig. 6

XBB 792-1498

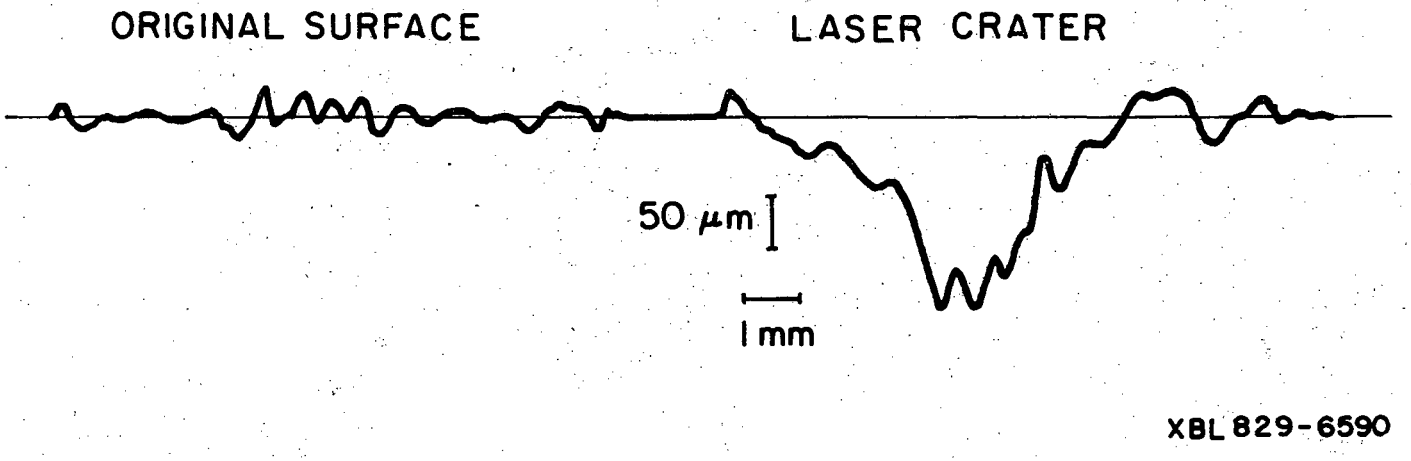

Fig. 7

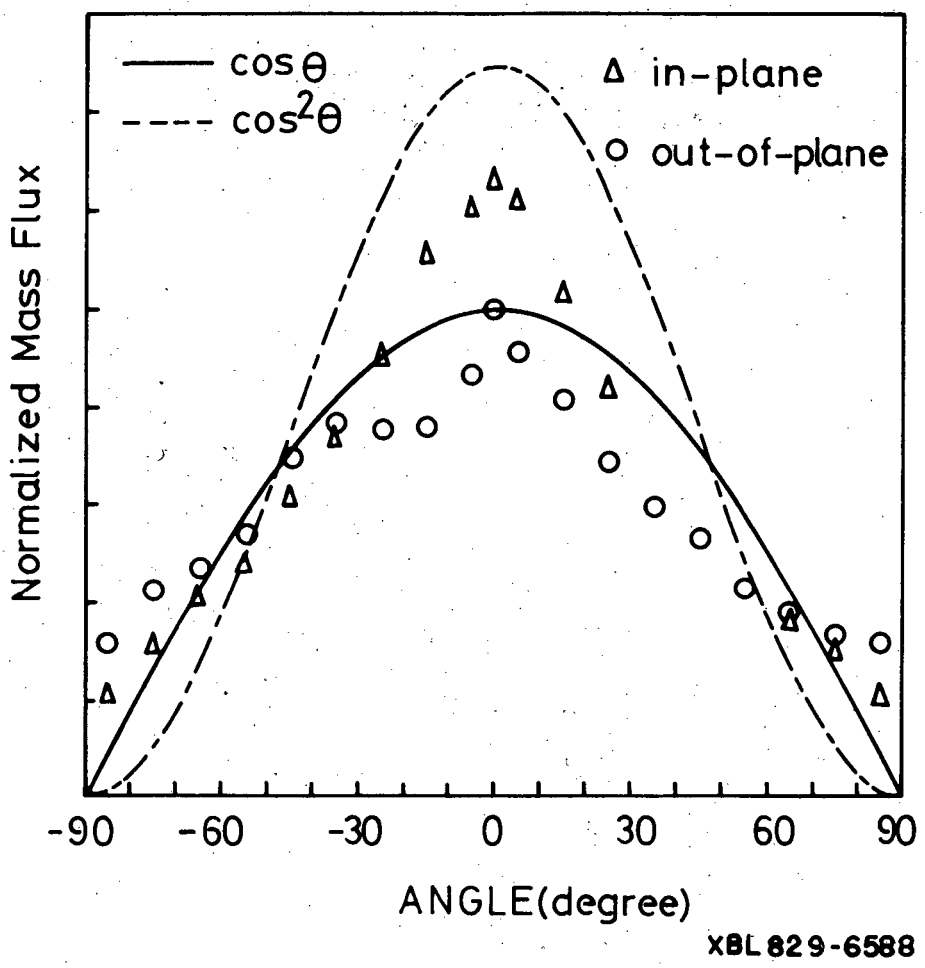
cosθ
cos²θ
Δ in-plane
O out-of-plane
Normalized Mass Flux
-90
-60
-30
0
30
60
90
ANGLE(degree)
XBL829-6588

Fig. 8

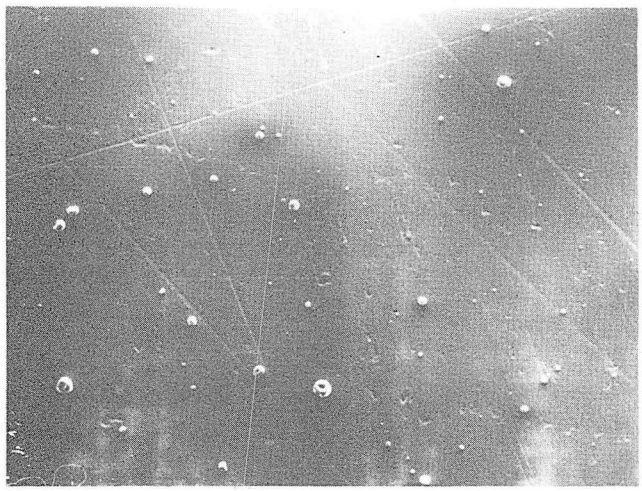

(a)

100 μm

(b)

10 μm

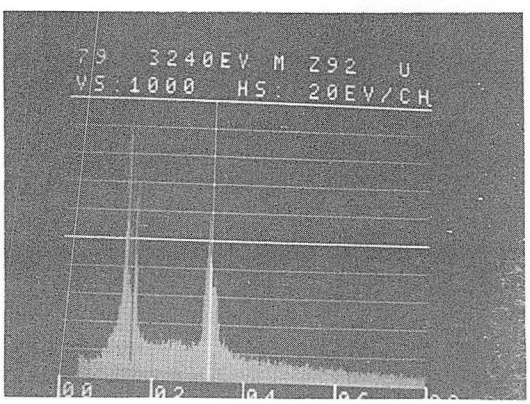

(c)

Aℓ U

Fig. 9

XBB 792-1497

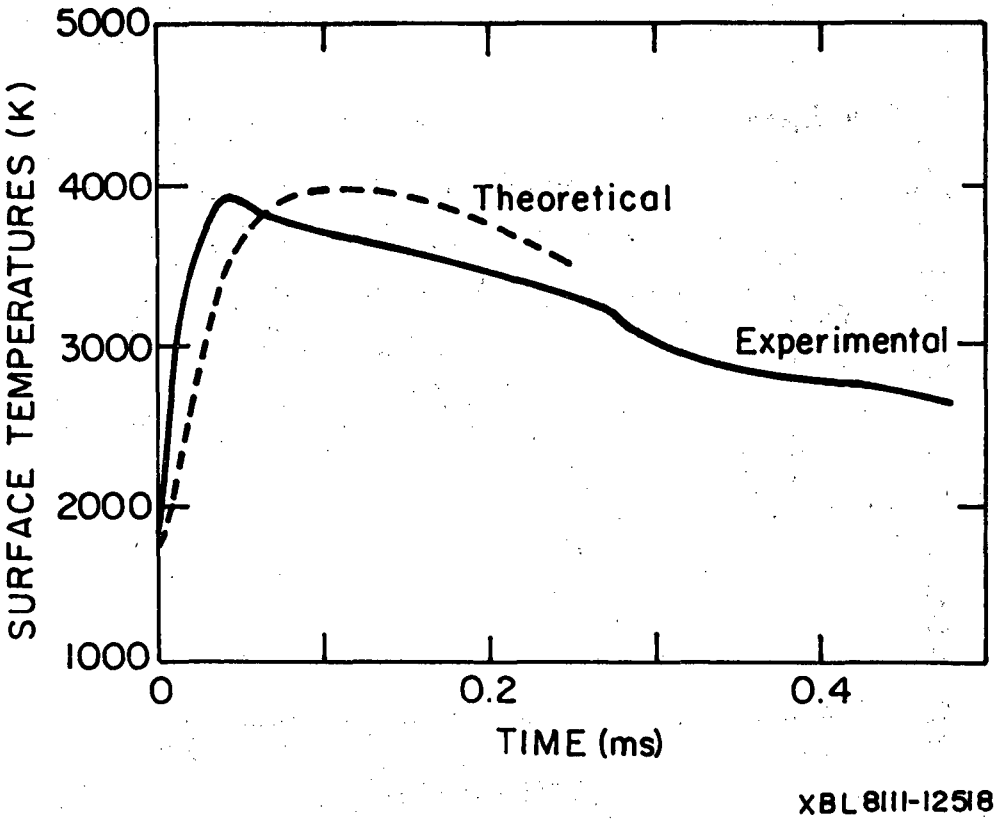
5000
4000
3000
2000
1000
SURFACE TEMPERATURES (K)
Theoretical
Experimental
0
0.2
0.4
TIME (ms)
XBL 8111-12518

Fig. 10

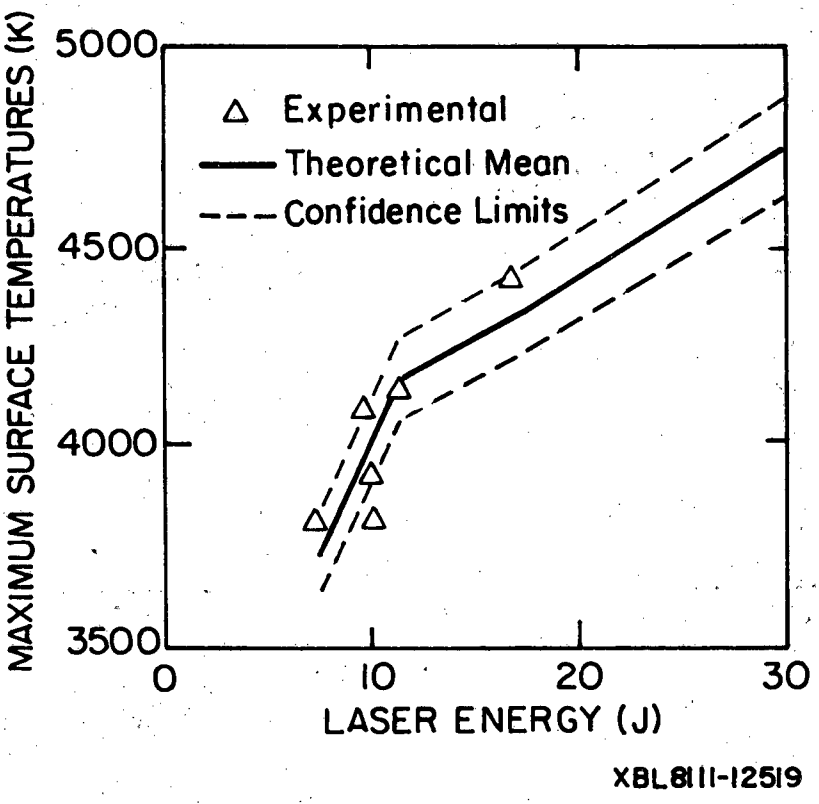
MAXIMUM SURFACE TEMPERATURES (K)
5000
4500
4000
3500
0
10
20
30
LASER ENERGY (J)
Experimental
Theoretical Mean
Confidence Limits
XBL8111-12519

Fig. 11

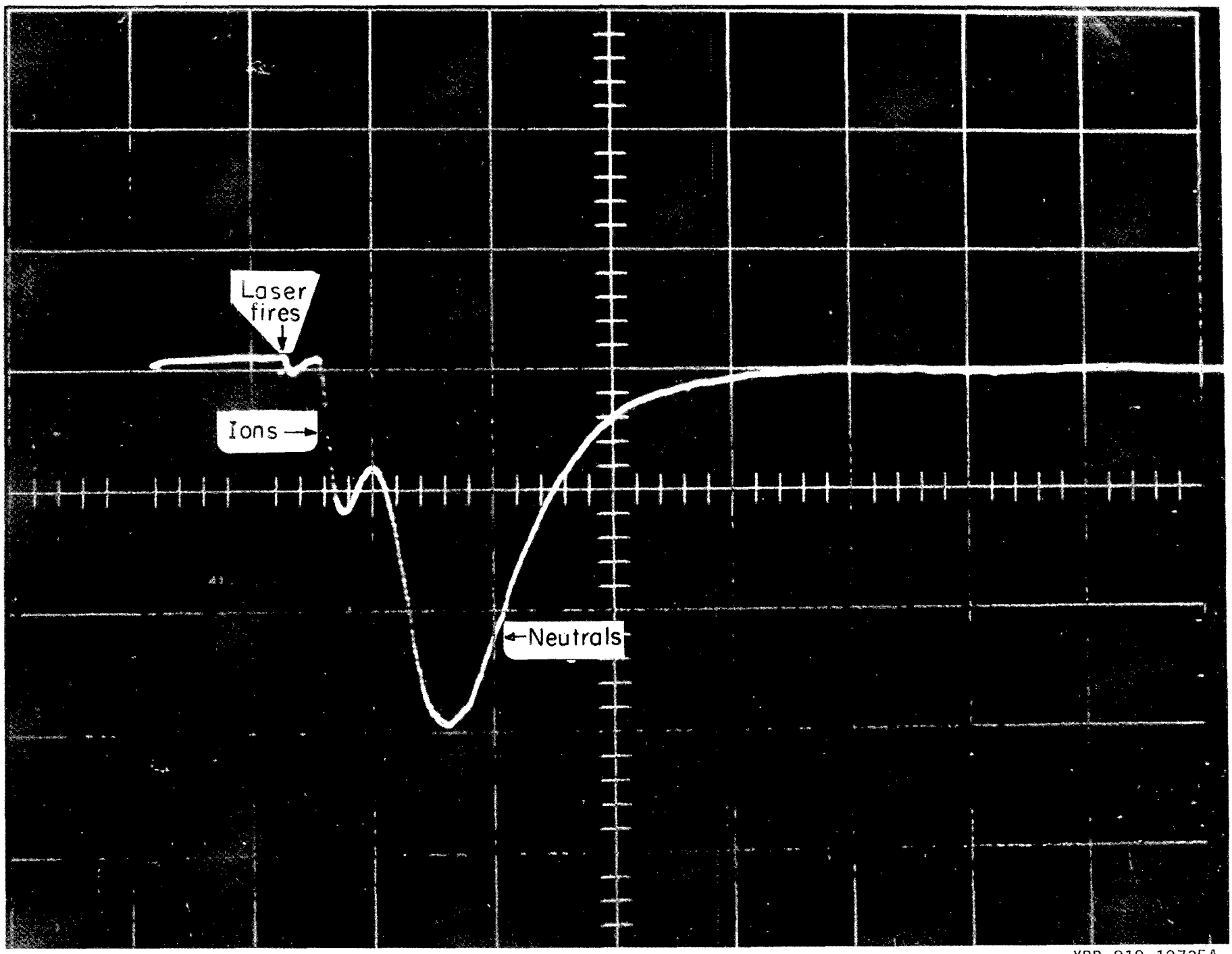

XBB 810-10735A

Fig. 12

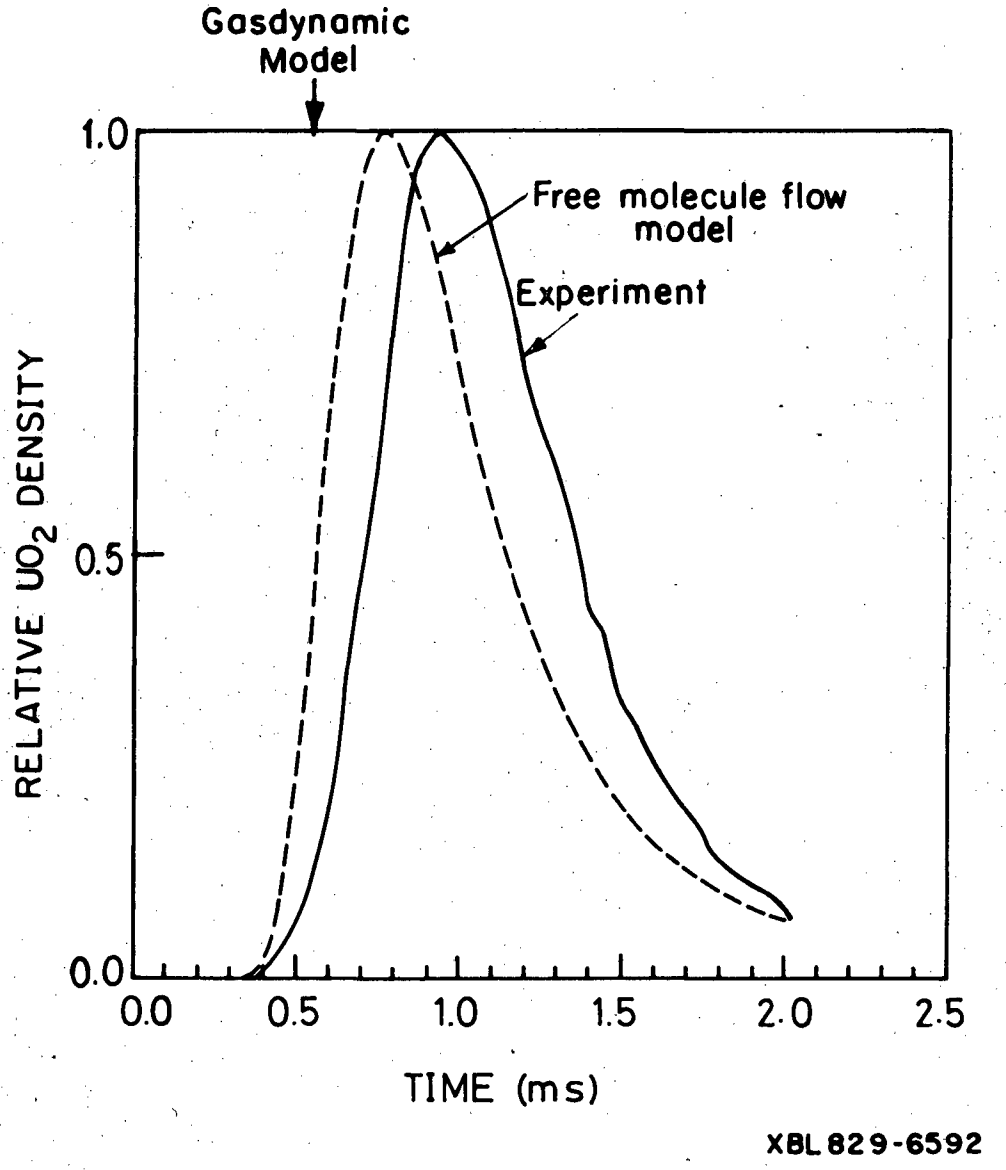
Gasdynamic
Model
1.0
0.5
0.0
RELATIVE UO_2 DENSITY
Free molecule flow
model
Experiment
0.0
0.5
1.0
1.5
2.0
2.5
TIME (ms)
XBL829-6592

Fig. 13

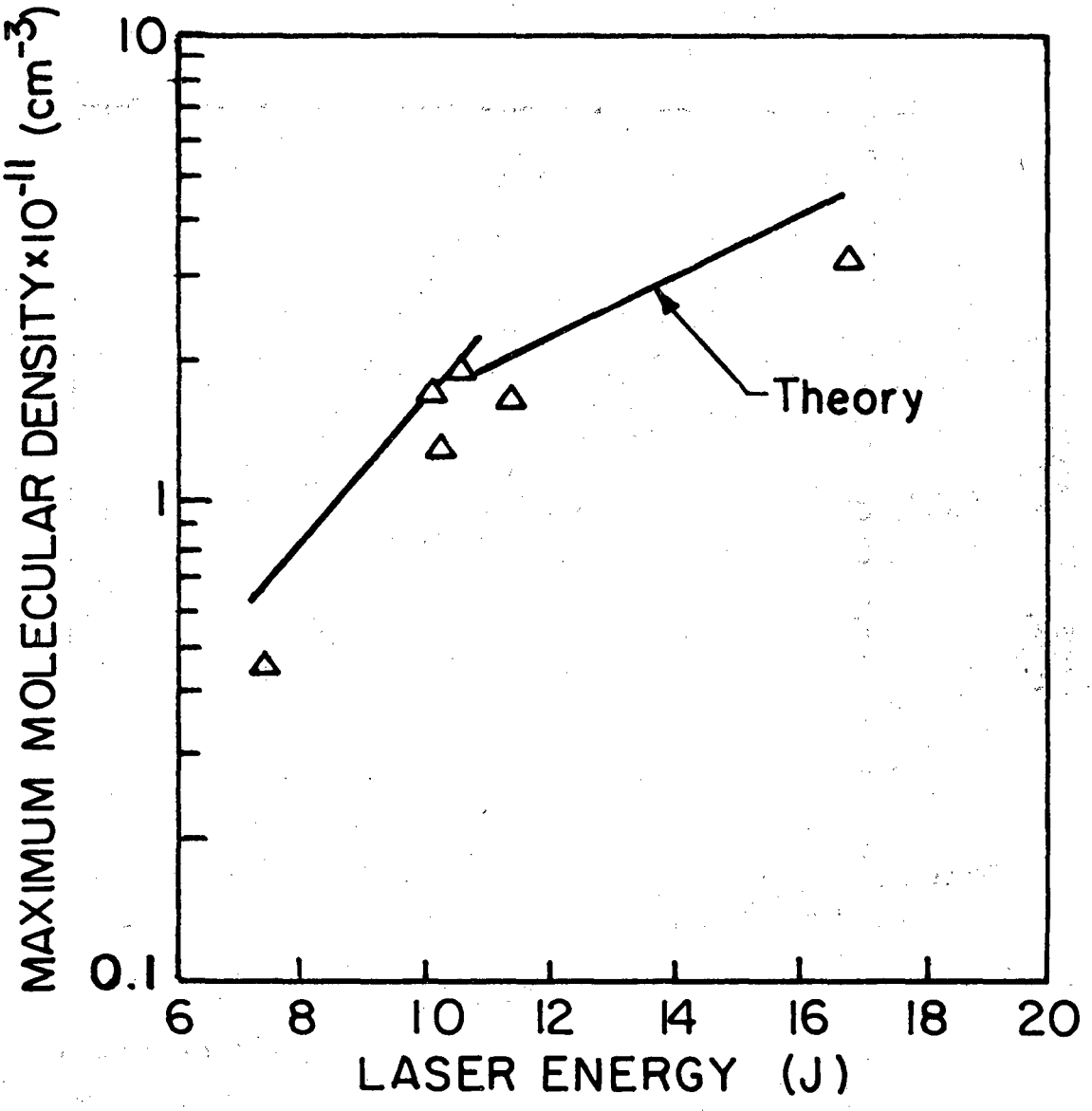
MAXIMUM MOLECULAR DENSITY×10⁻¹¹ (cm⁻³)
10
1
0.1
6
8
10
12
14
16
18
20
LASER ENERGY (J)
Theory
XBL 8210-6766

Fig. 14

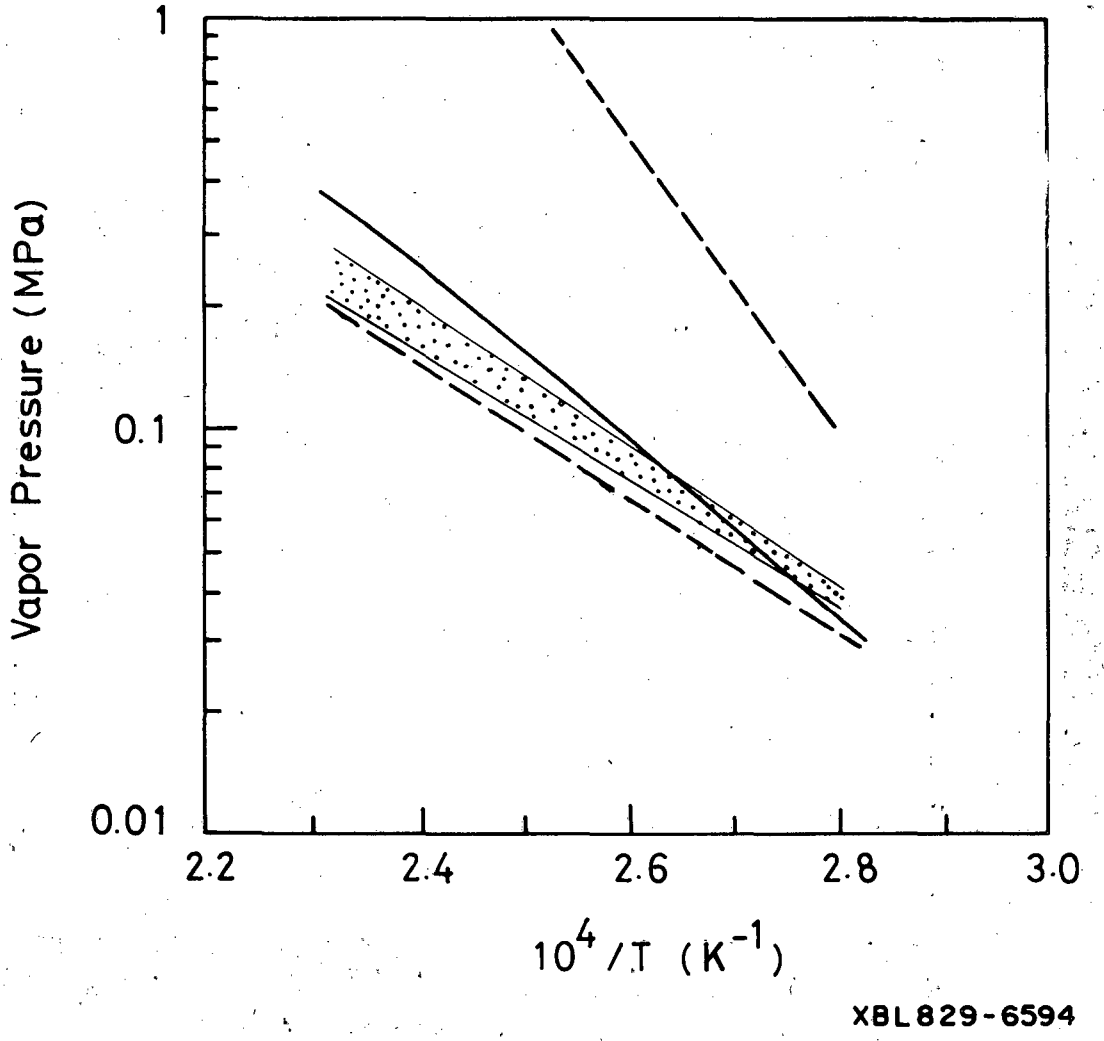

Fig. 15

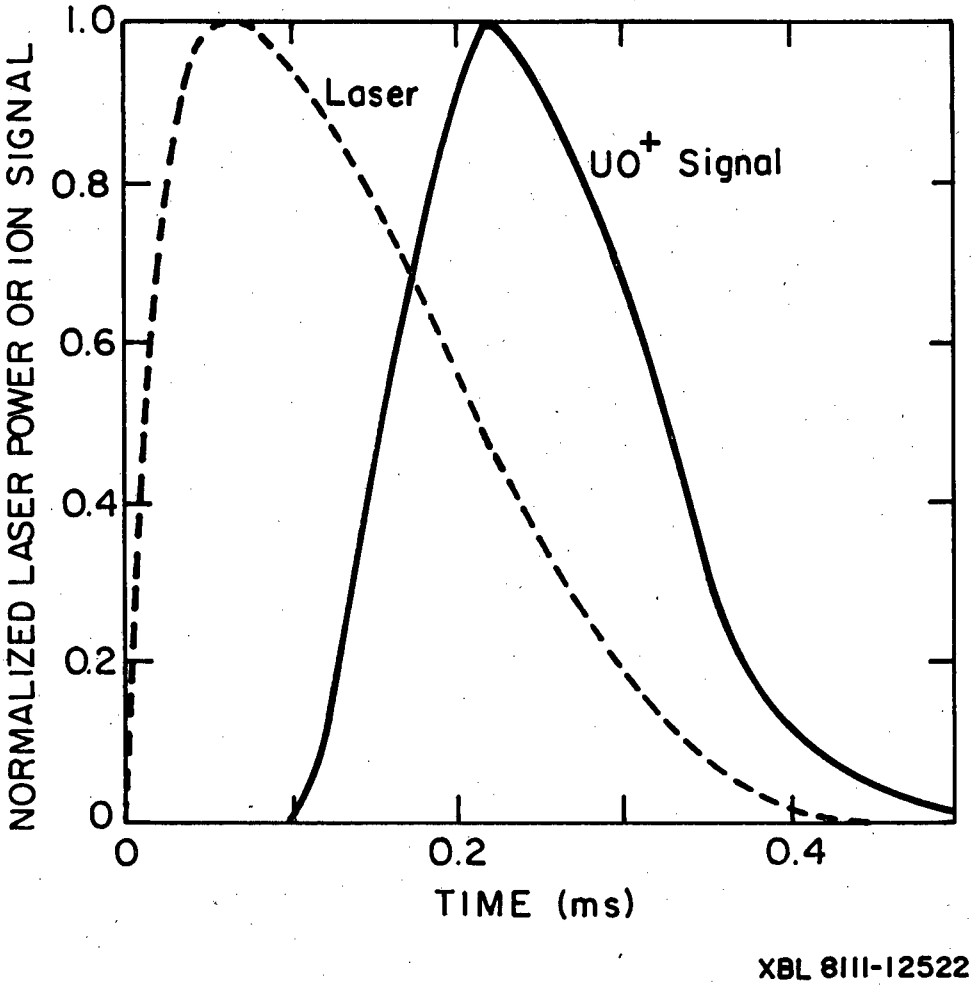
NORMALIZED LASER POWER OR ION SIGNAL
1.0
0.8
0.6
0.4
0.2
0
Laser
UO^+ Signal
0
0.2
0.4
TIME (ms)
XBL 8111-12522

Fig. 16

TECHNICAL INFORMATION DEPARTMENT
LAWRENCE BERKELEY LABORATORY
UNIVERSITY OF CALIFORNIA
BERKELEY, CALIFORNIA 94720